

VGS31b: a highly inclined ring along a filament in a void. Implication for the cold accretion.

M. Spavone^{1*}, E. Iodice²

¹*Dipartimento di Fisica e Astronomia, Università di Padova, Vicolo dell'Osservatorio 2, I-35122 Padova, Italy*

²*INAF-Astronomical Observatory of Naples, via Moiariello 16, I-80131 Napoli, Italy*

Accepted 2013 July 5. Received 2013 July 1; in original form 2013 May 21

ABSTRACT

VGS31b is a highly-inclined ring galaxy found along a filament in a void (Kreckel et al. 2012). Detailed photometry, by using u , g , r , i , z SDSS images, has shown that the overall morphology of VGS31b is very tricky, due to *i*) the presence of a highly inclined (72°) ring-like structure, which reaches the galaxy center tracing a “spiral-like” pattern, *ii*) a one sided tail towards North-East and *iii*) a bar in the central regions (Beygu et al. 2013). Such structure is reasonably the result of a “second event” in the evolution history of this galaxy, which could be a gravitational interaction with a companion galaxy or with the environment.

The main aim of the present work is to address the most reliable formation scenario for this object, by comparing the observed properties, i.e. structure, baryonic mass, kinematics and chemical abundances, with the theoretical predictions. In particular, we have used archival spectroscopic data, to derive the metallicity in the ring: we found a very low, sub-solar average value of $Z = 0.3Z_\odot$, comparable with other polar ring/disk galaxies, but lower than those measured for ordinary spirals of similar luminosity. The study of the chemical abundances in polar ring/disk galaxies and related objects has received an increasing attention in recent years, since it has revealed to be a key-parameter to disentangle among the formation scenarios suggested for this class of objects: major merging, tidal accretion or cold accretion. In the present work we check the cold accretion of gas through a “cosmic filament” as a possible scenario for the formation of the ring-like structure in VGS31b.

Key words: Galaxies: abundances – Galaxies: evolution – Galaxies: formation – Galaxies: individual: MRK1477 – Galaxies: peculiar – Methods: data analysis.

1 INTRODUCTION

The formation and evolution of galaxies is one of the leading themes of the modern observational cosmology. There are three main scenarios proposed for galaxy formation: 1) the monolithic collapse (Eggen et al. 1962), in which the collapse of the initial gas clouds quickly form stars leading to the formation of spheroidal systems, while the disks form later on through gas accretion; 2) the hierarchical scenario, in which disks are the first to form and then interactions and mergers lead to the formation of spheroids; 3) the external gas accretion from filaments (Combes 2011), in which disks form first and may evolve without merger with other galaxies, forming spheroids at the center through secular evolution acquiring gas from cosmic web filaments.

The advent of new all-sky surveys and high resolution data, covering a wide wavelength range, have strongly confirmed that gravitational interactions and mergers affect the morphology and dynamics of galaxies at all redshifts. In this framework, the study of peculiar and interacting galaxies can shed light on the main processes at work during galaxy interactions and on the influence of their environment. However, how galaxies acquire their gas is still an open issue in the models of galaxy formation. Recent theoretical works, which are supported by many numerical simulations, have argued that cold accretion plays a major role (Katz & White 1993; Katz et al. 1994; Kereš et al. 2005; Dekel & Birnboim 2006; Dekel & Birnboim 2008; Bournaud & Elmegreen 2009). Kereš et al. (2005) studied the physics of the *cold mode* of gas accretion in detail and they find that it is generally directed along filaments, allowing galaxies to draw gas from large distances. In particular,

* E-mail: spavone@na.astro.it (MS)

the cold accretion is a key mechanism for providing gas to disk galaxies (Brosch et al. 2010).

Recent simulations of disk formation in a cosmological context, performed by Agertz et al. (2009), revealed that the so-called chain galaxies and clump clusters, found only at higher redshifts (Elmegreen et al. 2007), are a natural outcome both of early epoch enhanced gas accretion from cold dense streams and of tidally and ram-pressured stripped material from minor mergers and satellites. This freshly accreted cold gas settles into large disk-like systems. This scenario reproduces the observed morphology and global rotation of disks and predicts both a realistic metallicity gradient and a star formation rate (SFR) of $20M_{\odot}/yr$. Agertz et al. (2009) find solar metallicity for the inner disk, while in the clump forming region it is only $\sim 1/10Z_{\odot}$, owing to the accretion of pristine gas in the cold streams mixed with stripped satellite gas.

Simulations also show that the interaction region between the newly formed disk and the cold streams can also cause it to be misaligned with the initial galactic disk. Based on very limited statistics, Agertz et al. (2009) suggest that this misalignment might not be typical, and that it comes from a third cold stream that is perpendicular to the main filament. More recent analysis shows that the accretion of gas along misaligned filaments with respect to the disk plane are more common, and it leaves traces down to low redshift (Dekel et al. 2009; Roškar et al. 2010). An almost polar structure can result even as an extreme case of this process and, as suggested by Agertz et al. (2009), it could be responsible for forming polar disks.

Hydrodynamical simulations performed by Macciò et al. (2006) and Brook et al. (2008) have shown that the formation of a polar disk galaxy can occur naturally in a hierarchical universe, where most low-mass galaxies are assembled through the accretion of cold gas infalling along filamentary structures. According to Macciò et al. (2006), the polar disk forms from cold gas that flows along the extended $\sim 1Mpc$ filament into the virialized dark matter halo. The gas streams into the center of the halo on an orbit that is offset from radial infall. As it reaches the center, it impacts with gas in the halo of the host galaxy and with the warm gas flowing along the opposite filament. Only the gas accreted perpendicular to the major axis of the potential can survive for more than a few dynamical lifetimes.

Brook et al. (2008) argue that polar disk galaxies are extreme examples of the misalignment of angular momentum that occurs during the hierarchical structure formation: an inner disk starts forming shortly after the last major merger at $z \sim 2$. Because of its gas rich nature, the galaxy rapidly forms a new disk whose angular momentum is determined by the merger orbital parameters. Later, gas continues to be accreted but in a plane that is almost perpendicular to the inner disk. At $z \sim 0.8$ the central galaxy is still forming stars in a disk, while the bulk of new star formation is in a highly inclined polar disk. The inner disk has exhausted its gas by $z \sim 0.5$, while gas continues to fall onto the polar disk. From this point on, star formation occurs exclusively in the polar disk, which remains stable for at least 3 Gyrs. The formation mechanisms described above can self-consistently explain both the morphology and kinematics of a polar disk galaxy.

The observed similarities between polar ring/disk galaxies, i.e. structure, gas content, age, (Arnaboldi et al. 1997; Iodice et al. 2002; Cox et al. 2006; Spavone et al. 2010, 2011) and similar formation history with disk galaxies, yield in the latest decade, a renewed effort in studying the morphology and kinematics of Polar Ring/Disk Galaxies (PRGs). These systems are made by a central spheroidal component and a polar structure of gas, stars and dust (Whitmore et al. 1990): the existence of two orthogonal components of the angular momentum is a consequence of a second event in their formation history. They can thus be considered an ideal laboratory to study the physics of accretion/interaction mechanisms, the disk formation and the dark halo shape.

Recent studies on the prototype of PRGs, NGC4650A, revealed that the polar structure in this object has disk-like morphology and kinematics, rather than the nature of a ring (see Arnaboldi et al. 1997; Iodice et al. 2002; Gallagher et al. 2002; Swaters & Rubin 2003). Since then, theoretical predictions have been re-addressed to understand how different kinds of galaxy-galaxy and galaxy-environment interactions lead to different morphologies and kinematics of PRGs and in particular, if galaxies with “pure rings” could form with the same mechanism that led to the growth of a polar disk.

Currently, in addition to the cold accretion scenario widely described above, the other two main formation processes proposed for accounting the PRGs manifold are: *i*) a major dissipative merger and the *ii*) tidal accretion of material (gas and/or stars) by a donor. In the merging scenario, the PRG results from a “polar” merger of two disk galaxies with unequal mass (Bekki 1998; Bournaud et al. 2005). In the accretion scenario, the polar ring/disk may form by a) the disruption of a dwarf companion galaxy orbiting around an early-type galaxy (ETG), or by b) the gas accretion on an ETG from the outskirts of a tidally stripped disk galaxy, during a parabolic encounter (Reshetnikov & Sotnikova 1997; Bournaud & Combes 2003; Hancock et al. 2009).

Recent observational studies on PRGs (Iodice et al. 2006; Spavone et al. 2010, 2011) single out the critical physical parameters that allow to disentangle among the formation scenarios. They are 1) the total baryonic mass of the polar structure vs. that of central spheroid; 2) the kinematics along both the equatorial and meridian planes; 3) the metallicity & SFR in the polar structure. By studying the chemical abundances in the polar structure of three polar ring/disk galaxies, NGC4650A, UGC7576 and UGC9796, Spavone et al. (2010, 2011) have led the way in implementing a test for the cold accretion, tracing the formation history of these objects by accounting for all the three parameters mentioned above. In particular, the low, sub-solar metallicities derived for these objects turn to be consistent with the estimates for a simulated polar disk galaxy formed via cold accretion (Snaith et al. 2012).

In this work, we would like to perform the same kind of analysis on the galaxy VGS31b, which is a highly-inclined ring galaxy found along a filament in a void (Kreckel et al. 2012). Main aim of the present work is to address the most reliable formation scenario for this object, by comparing the observed properties, i.e. structure, baryonic mass, kinematics and chemical abundances, with the theoretical predictions.

The paper has the following structure: in Sec.2 are described the main properties of VGS31b, in Sec.3 we describe the data reduction and analysis, in Sec.4 and 5 we show the results of the photometric analysis. In Sec.6, 7 and 8 we describe the study of the chemical abundances of VGS31b, while discussion and conclusions are illustrated in Sec.9.

2 PROPERTIES OF VGS31

VGS31 (Figure 1) is a system of three aligned galaxies belonging to a multiwavelength survey of 60 void galaxies, called “The Void Galaxy Survey” (VGS), conducted by Kreckel et al. (2012).

Beygu et al. (2013) show that the whole system is embedded in a common HI envelope and the three galaxies have almost the same velocity. They also assert that the absence of a velocity gradient throughout the HI envelope suggests that it is a filament in which the three galaxies are embedded. VGS31 consists of a central galaxy VGS31a and two companions, VGS31b at the far east side and VGS31c at the far west side, and shows strong signs of interaction.

VGS31b is the most disturbed object of this small group; it is at a distance of about 84 Mpc, based on $H_0 = 75 \text{ km s}^{-1} \text{ Mpc}^{-1}$ and has a heliocentric radial velocity of $V = 6218 \text{ km s}^{-1}$, which implies that 1 arcsec = 0.4 kpc. VGS31b is a starburst Markarian galaxy (MRK1477) with a one sided tail, curved toward north-east, kinematically connected to the central early-type disk galaxy (HG), a ring-like structure around the HG and a fast rotating inner structure with streaming motions characteristic of a bar. Both the tail and the ring are not detected in $H\alpha$ or UV, but are clearly visible in optical and HI. Moreover, Beygu et al. (2013) also found that among the three galaxies, VGS31b has higher SFR_α .

The central HG have a diameter of ~ 41 arcsec (~ 16 kpc), while the ring-like structure is more extended than the optical disk, having a diameter of ~ 60 arcsec (~ 24 kpc).

3 OBSERVATION AND DATA REDUCTION

3.1 Spectroscopic data

The long slit spectra analyzed in this work are archival data, obtained with ISIS@WHT (Intermediate dispersion Spectrograph and Imaging System) on May 2011 under the program ID. N20. ISIS is mounted at the Cassegrain focus of the 4.2m William Herschel Telescope and is a high-efficiency, double-armed, medium-resolution ($8\text{-}120 \text{ \AA mm}^{-1}$) spectrograph. Use of dichroic slides permits simultaneous observing in both blue and red arms, which are optimised for their respective wavelength ranges. The dataset studied in this work is the same presented by Beygu et al. (2013), made by long-slit spectra acquired along two different Position Angles (P.A.), $P.A. = 230^\circ$ and $P.A. = 158^\circ$, corresponding to the central spheroidal galaxy and the outer ring directions, respectively. These data were used by Beygu et al. (2013) to estimate the Star Formation Rate from the $H\alpha$ luminosity. The main goal of the present study is to estimate the metallicity in the ring-like structure of VGS31b, thus we have analyzed only the spectra relative to this component, acquired with a slit $1''$ wide and aligned at $P.A. = 158^\circ$.

At the systemic velocities of VGS31b, to cover the red-shifted emission lines of $[OII]\lambda 3727$, $H\gamma(\lambda 4340)$, $[OIII]\lambda 4363$, $[OIII]\lambda\lambda 4959, 5007$, $H\beta(\lambda 4861)$ and $H\alpha(\lambda 6563)$, the gratings R600B and R1200R for the blue and the red arm were used, with a resolution of 0.45 and $0.26 \text{ \AA pix}^{-1}$ respectively.

The data reduction was carried out using the CCDRED package in the IRAF¹ (*Image Reduction and Analysis Facility*) environment. The main strategy adopted for each dataset included dark subtraction², flat-fielding correction, sky subtraction, and rejection of bad pixels. Wavelength calibration was achieved by means of comparison spectra of CuNe+CuAr lamps acquired for each observing night, using the IRAF TWODSPEX.LONGSLIT package. The sky spectrum was extracted at the outer edges of the slit, for $r \geq 30$ arcsec from the galaxy center, where the surface brightness is fainter than 24 mag/arcsec^2 , and subtracted off each row of the two dimensional spectra by using the IRAF task BACKGROUND in the TWODSPEX.LONGSLIT package. On average, a sky subtraction better than 1% was achieved. The sky-subtracted frames were co-added to a final median-averaged 2D spectrum.

The final step of the data processing is the flux calibration of each 2D spectrum, by using observations of the standard star BD284211 and the standard tasks in IRAF (STANDARD, SENSFUNC and CALIBRATE). To perform the flux calibration, we extracted a 1-D spectrum of the standard star to find the calibration function, and then we extracted a set of 1-D spectra of the galaxy by summing up a number of lines corresponding to the slit width. Since the slit width was $1''$ and the scale of the instrument was $0.19''/\text{pix}$, we collapsed five lines to obtain each 1-D spectrum. Finally we applied the flux calibration to this collection of spectra, showed in Fig.2.

The fluxes of these emission lines were measured using the IRAF SPLOT routine, which provides an interactive facility to display and analyze spectra. We evaluated the flux and equivalent width by marking two continuum points around the line to be measured. The linear continuum is subtracted and the flux is determined by simply integrating the line intensity over the local fitted continuum. The errors on these quantities are calculated, following Pérez-Montero & Díaz (2003), by the relation $\sigma_1 = \sigma_c N^{1/2} [1 + EW/(N\Delta)]^{1/2}$, where σ_1 is the error in the line flux, σ_c the standard deviation in a box near the measured line and represents the error in the continuum definition, N is the number of pixels used to measure the flux, EW the equivalent width of the line, and Δ the wavelength dispersion in $\text{\AA}/\text{pixel}$.

3.1.1 Reddening correction

Reduced and flux-calibrated spectra and the measured emission line intensities were corrected for the reddening, which account both for that intrinsic to the source and to the

¹ IRAF is distributed by the National Optical Astronomy Observatories, which is operated by the Associated Universities for Research in Astronomy, Inc. under cooperative agreement with the National Science Foundation.

² Bias frame is included in the dark frame.

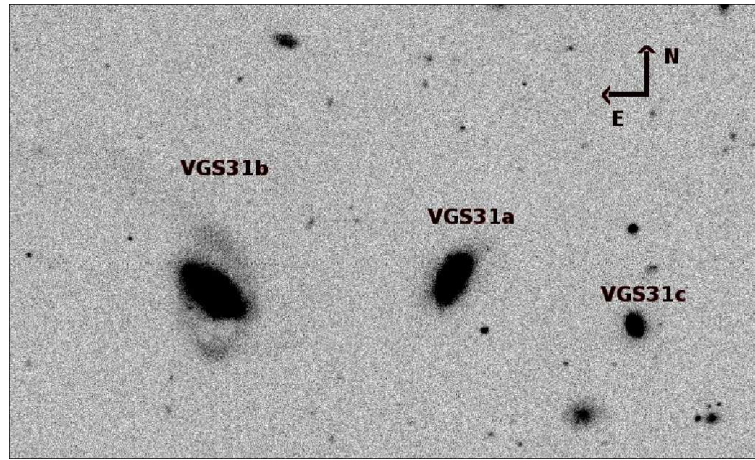


Figure 1. SDSS g-band image of the galaxy group VGS31.

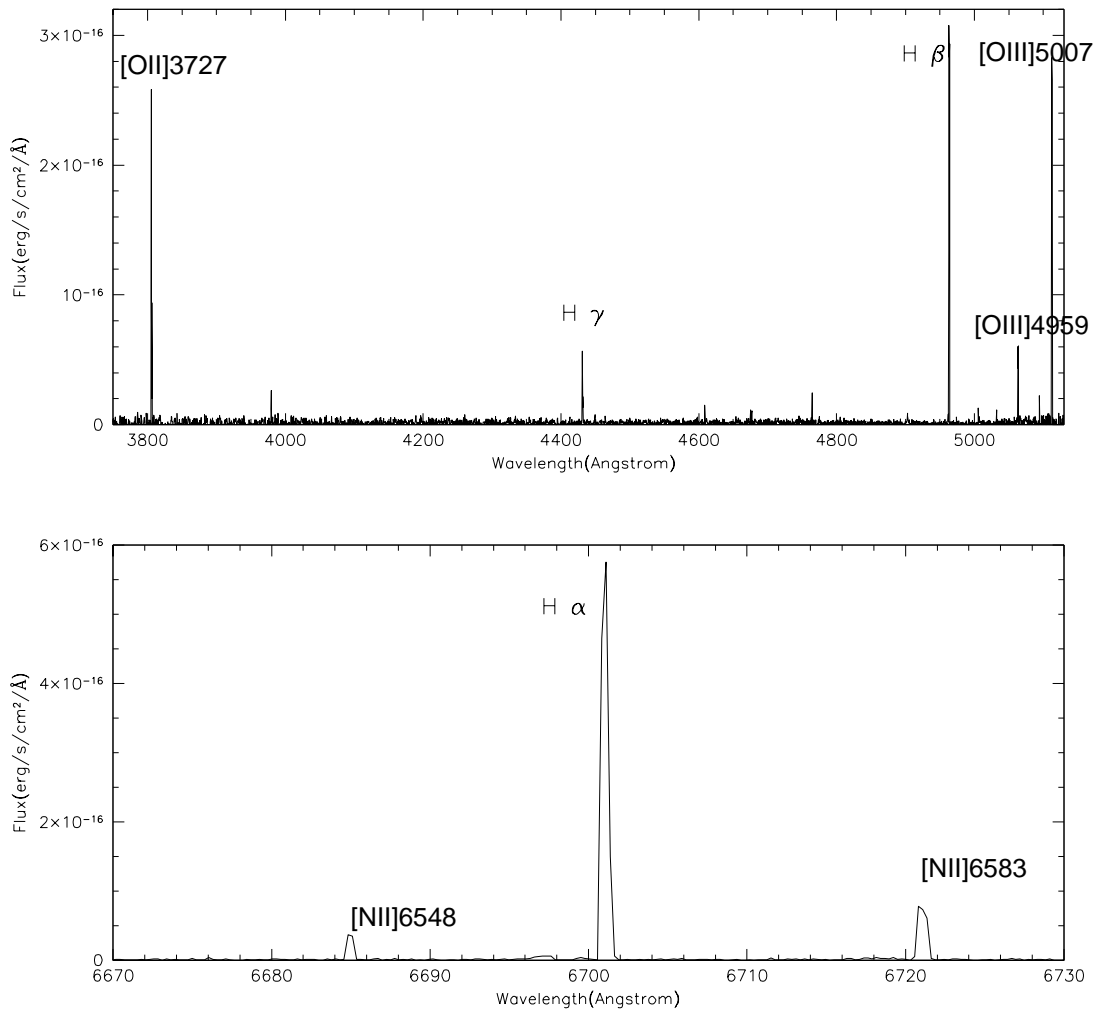


Figure 2. 1D spectra of VGS31b corresponding to a line extracted at a distance of ~ 20 arcsec from the galaxy center.

Milky Way. By comparing the intrinsic Balmer decrement $H\alpha/H\beta = 2.89$, we derived the visual extinction $A(V)$ and the color excess $E(B - V)$ by adopting the mean extinction curve by Cardelli et al. (1989) $A(\lambda)/A(V) = a(x) + b(x)R_V$, where $R_V \equiv A(V)/E(B - V) = 3.1$ and $x = 1/\lambda$. All the emission lines in the spectra of VGS31b are in the *optical/NIR* range (see Cardelli et al. 1989), so we used the average R_V -dependent extinction law derived for these intervals to perform the reddening correction.

We derived the average observed Balmer decrements for the galaxy, which are

$$(H\alpha/H\beta) = 0.74 \pm 0.67$$

$$(H\gamma/H\beta) = 1.21 \pm 0.74,$$

while the color excess obtained by using these observed decrements are

$$[E(B - V)]_{H\alpha} = -1.34 \pm 0.39$$

$$[E(B - V)]_{H\gamma} = -1.87 \pm 0.26.$$

The negative value of the color excess indicates the presence of stars that are bluer and hotter than normal, and thus they have V apparent magnitude greater than the B one, leading to a negative B-V color. In general, stars hotter than Vega, which have $E(B - V) = 0$, have negative color excess (Masana et al. 1998).

Such values of $E(B-V)$ are used to derive the extinction A_λ through the Cardelli's law. Finally, the corrected fluxes are given by the following equation and listed in Tab.2.

$$\frac{F_{int}^\lambda}{F_{int}^{H\beta}} = \frac{F_{obs}^\lambda}{F_{obs}^{H\beta}} 10^{0.4[A_\lambda - A_{H\beta}]}. \quad (1)$$

3.2 Photometric data

We used SDSS images of VGS31 observed with a 2.5 meters telescope in the u , g , r , i , z bands. The field of view was 3 square degrees, with a pixel scale of 0.396 arcsec/pixel and an exposure time of about 53 seconds.

The ring-like structure of the galaxy is clearly visible in the g , r and i bands, while it disappears in the u and z bands (see Fig. 3).

4 HOST GALAXY AND RING MORPHOLOGY

The SDSS images of VGS31b (see Fig. 3) show that most of the galaxy light comes from the central HG, which has the morphology of an early-type disk galaxy and an average diameter of ~ 16 kpc. The ring-like structure, visible along the North-South direction, with a diameter of about 24 kpc, is more extended in radius than the host galaxy. The ring is clearly visible in the g , r and i bands, while it is not detectable in the u and z bands, and it appears knotty and dusty.

To emphasize the galaxy substructure, we create a residual image produced by taking the ratio of the original reduced g -band image with a smoothed one. We use the IRAF task FMEDIAN to smooth the original reduced image, by using a window size of 11×11 , that is chosen to best emphasize the inner structure of the central host. The final un-sharp masked image of VGS31b is shown in Fig.4: here, the complex structure of this galaxy, even in the very central regions, stands out very clear. We can identify two main features: *i*) a luminous bar-like structure which crosses the

center of the galaxy, along NE-SW direction, $P.A. \sim 230^\circ$ (see also Sec.5), and *ii*) two very luminous blobs observed in the NE and SW sides of the bar. Such features are also detected in the g -band light profiles (see Figure 8). Moreover, there are other two fainter substructures, almost parallel to the central luminous bar-like features, which appear as two arcs that connect the edges of the bar; that on the NE side appear more knotty, suggesting the presence of possible star-forming regions. On the other hand, the outer ring-like structure appears very smooth. The two bright blobs seem to be the ‘‘starting-point’’ of the two arms of the ring, since they are located on the same apparent ellipse (see Fig.4). The two inner arcs seems to connect the above features to the galaxy center by tracing a ‘‘spiral-like’’ pattern.

5 PHOTOMETRY: LIGHT AND COLOR DISTRIBUTION

A quantitative photometry of VGS31b has been performed by using all the SDSS bands (see Sec.3) in order derive the total light and typical scale-lengths of the main components observed in VGS31b (host galaxy and ring), to locate the inner substructure and, where possible, to estimate their contribution to the total light. To this aim, in the following sections we describe the isophotal analysis and light distribution.

5.1 Isophotal analysis

We used the IRAF-ELLIPSE task on the SDSS images to perform the isophotal analysis for VGS31b and the results are shown in Figure 5. The average surface brightness extends up to about 31 arcsec from the galaxy center for the g , r and i bands, while the u and z bands are less extended, reaching 18 and 28 arcsec respectively; the half-light radius is $R_e = 8.3$ arcsec in the u and g bands, and $R_e = 9.1$ in the r , i and z ones.

For a semi-major axis r , in the range $0 \leq r \leq 8$ arcsec, the Position Angle (P.A.) is almost constant and equal to $\sim 70^\circ$, indicating that in this regions the isophotes are almost coaxial; the ellipticity rises from 0.2 to 0.7, showing the presence of a flatter structure around 8 arcsec from the galaxy center. For $8 \leq r \leq 20$ arcsec the profiles reflect the presence of the ring and we observe a twisting of the isophotes of about 30° and lower values of the ellipticity ranging from 0.3 to 0.5. Finally, for $r \geq 20$ arcsec we observe another change in both ellipticity and P.A. with $\epsilon \sim 0.4$ and a twisting of $\sim 50^\circ$. At this radii the ellipticity and the P.A. are those of the isophotes corresponding to the ring-like structure, while in the range $0 \leq r \leq 8$ arcsec they correspond to the host galaxy. The difference between the P.A. of the central galaxy and of the ring-like structure is $\sim 70^\circ$, which is the relative inclination between host galaxy and ring. This difference turns to be consistent with that between the two P.A.s used to acquire the spectra along the two components, i.e. HG and ring, (see Sec. 3.1).

The ring-like structure affects the surface brightness profiles, in all bands, at least at three different distance from the galaxy center: at $r \sim 5$ arcsec, $r \sim 10.5$ arcsec, $r \sim 28$ arcsec, see Figure 6. These features turns to be much more

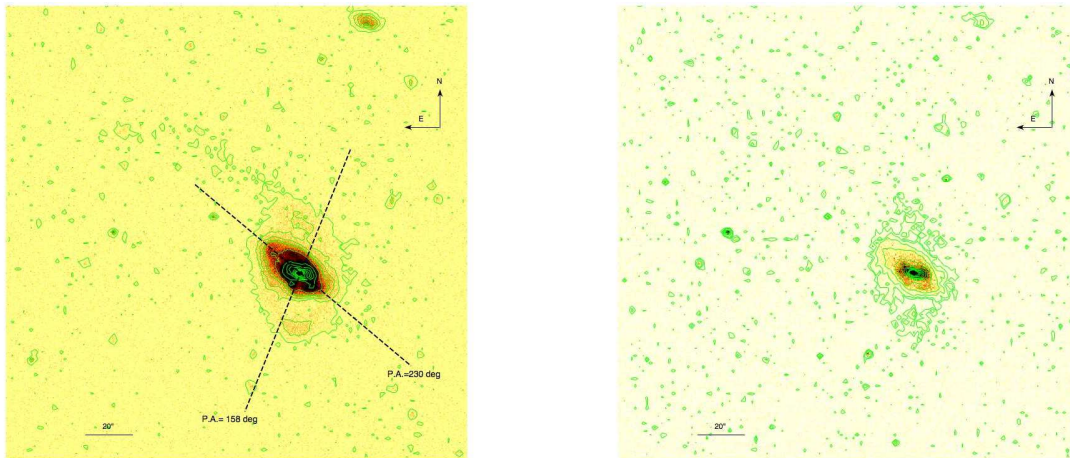


Figure 3. g band (left) and z band (right) images of VGS31b with, superimposed, the contour levels. The dashed lines correspond to the directions where the archive spectra are taken and where the light profiles have been extracted (see Sec.5.2).

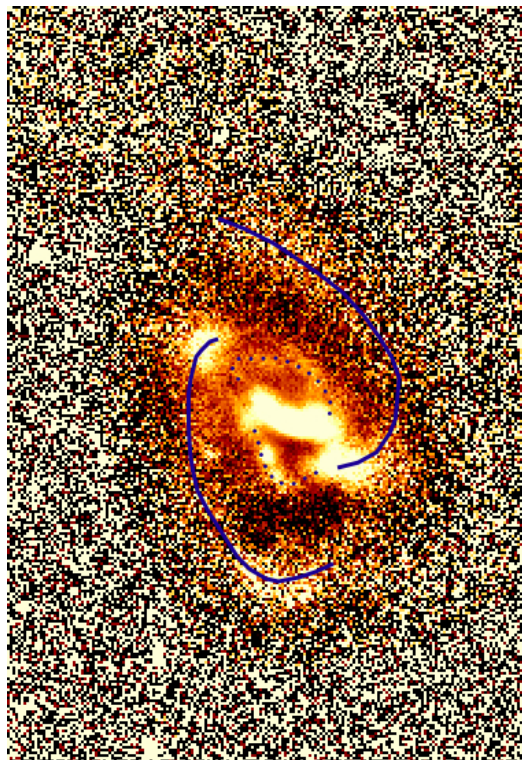


Figure 4. High frequency residual g band image for VGS31b. Lighter colors correspond to brighter features. The blue dotted and solid curves, highlight the two arcs connecting the edges of the central bar and the two arms of the ring, respectively. The north is up while the east is on the left.

evident in the light profiles extracted along the major axes of the two components (see Figures 8 and 9).

In order to analyze the complex structure of VGS31b, which is very luminous in the g band, we have also derived the 2D model in this band by using the IRAF task BMODEL. We have created a 2-dimensional model image from the results of the isophotal analysis generated by the isophote fitting task ELLIPSE and subtracted this model to the g band image, obtaining the residual image shown in Fig. 7. The residuals emphasize the presence of a very complex structure in this galaxy, as already shown by the un-sharp masked im-

age. In particular, also in this case we can identify the ring’s arms connected to the two bright blobs at the ends of the bar-like structure, and the “spiral-like” pattern traced by the ring up to the central regions of the galaxy.

5.2 Light and color distribution

In Figures 8 and 9 we show the light profiles in the g and i bands, respectively, along the HG and ring-like structure, $P.A. = 230$ and $P.A. = 158$ degrees respectively, at the same position angles used to acquire the spectra analyzed

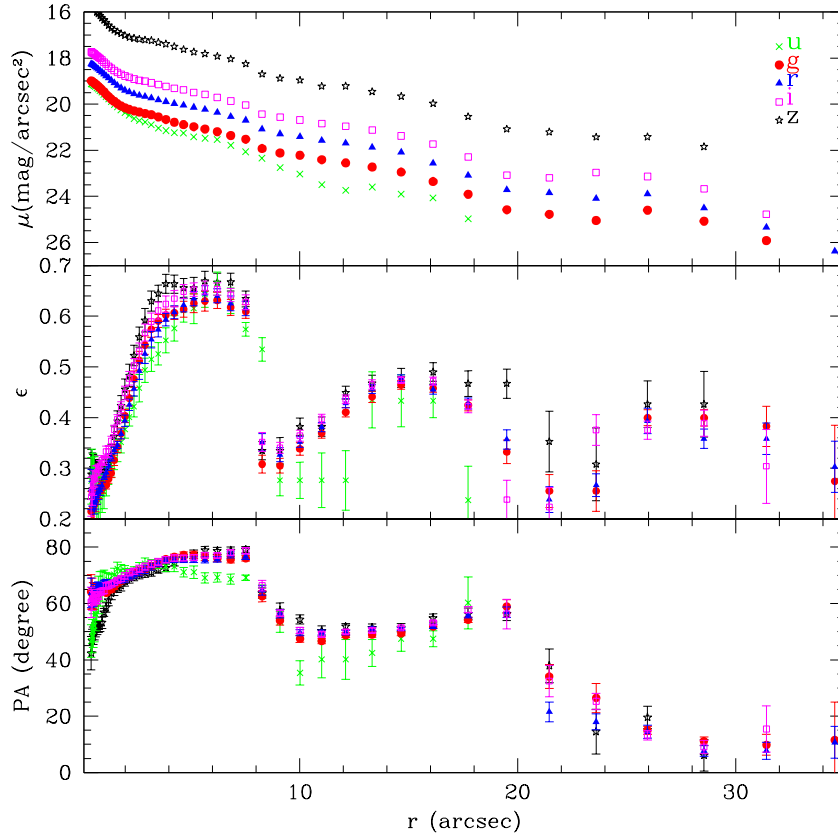


Figure 5. Position Angle (P.A.), Ellipticity (ϵ) and mean surface brightness profile in the u, g, r, i and z SDSS bands. The error bar for the surface brightness profile (± 0.04 for the u band, ± 0.01 for the g, r and i bands, and ± 0.02 for the z band) is within the dimensions of data points.

in this work (see Sec. 3.1 and Fig.3). From this point on, we refer as “major axis” of each component in VGS31b, i.e. HG and ring, the directions along the above two position angles. In both bands, along the HG major axis, the light profiles show a central bright concentration inside 4 arcsec, the three bright bumps, already identified in the average isophotal profiles (see Fig.6), located at $4 \leq R \leq 5$ arcsec and $10 \leq R \leq 18$ arcsec on the NE side, and at $R \sim 10$ arcsec on the SW side. The inner one, reflects the presence of the inner bar-like structure, while the other two ones, at a larger radii, are due to the bright blobs identified in Fig.4, which are probably connected to the ring. Along the ring major axis, light profiles are smoother, showing a behaviour typical for galaxies with rings (Iodice et al. 2002): two prominent bumps, at $4 \leq R \leq 8$ arcsec, are due to the ring light superimposed to the underlying HG light. Both the light distribution along the main axes of the galaxy and the previous analysis of the galaxy morphology (see Sec.5) show that the ring contributes to the galaxy light at several distances from the centre. Since we aim to derive an average estimate of the metallicity (Z) for the ring component, we modelled the underlying light distribution of the HG, in order to obtain the range of radii where the ring dominates with respect to the HG and derive the average value for Z. Such model of the light distribution of the only HG compo-

nent need to be performed by fitting the 1D light profiles, where is possible and easy to exclude the regions where the ring dominates, i.e. at $4 \leq R \leq 5$ arcsec and $10 \leq R \leq 18$ arcsec on the NE side, and at $R \sim 10$ arcsec on the SW side. The light distribution of the HG in VGS31b has been modelled by adopting a Sersic law $\mu[r] \propto \mu_e + (r/r_e)^{1/n}$ (Sérsic 1963), both in the g and in the i bands: results are shown in Figures 8 and 9. The best fit is obtained with $\mu_e = 22.3 \pm 0.1$, $r_e = 6.8 \pm 0.5$, $n = 3.0 \pm 0.1$, and suggests that: *i*) both along the HG and ring major axis (bottom and top panels, respectively), in the central regions, for $R \leq 5$ arcsec, the HG is the dominant component; *ii*) along the HG major axis (bottom panels), in the range $0.5 \leq R \leq 20$ arcsec, most of the light comes from the ring, while at larger distances, inside the scatter of the data, the light distribution follows the fitted Sersic law for the HG; *iii*) along $P.A. = 158^\circ$ (top panels), the ring is the dominant component in the light distribution at all distance for $R \geq 5$ arcsec.

We have also derived the g-i and g-r color profiles along the host galaxy and ring major axis (Figures 10 and 11) and the 2-dimensional color maps. On average, the central regions of the galaxy have bluer colors, with a maximum value of g-i $\sim 1.6 \pm 0.02$ for the host galaxy and $\sim 1 \pm 0.02$ for the ring, and g-r $\sim 0.7 \pm 0.02$ for the host galaxy and $\sim 0.6 \pm 0.02$ for the ring. Both color maps are characterized

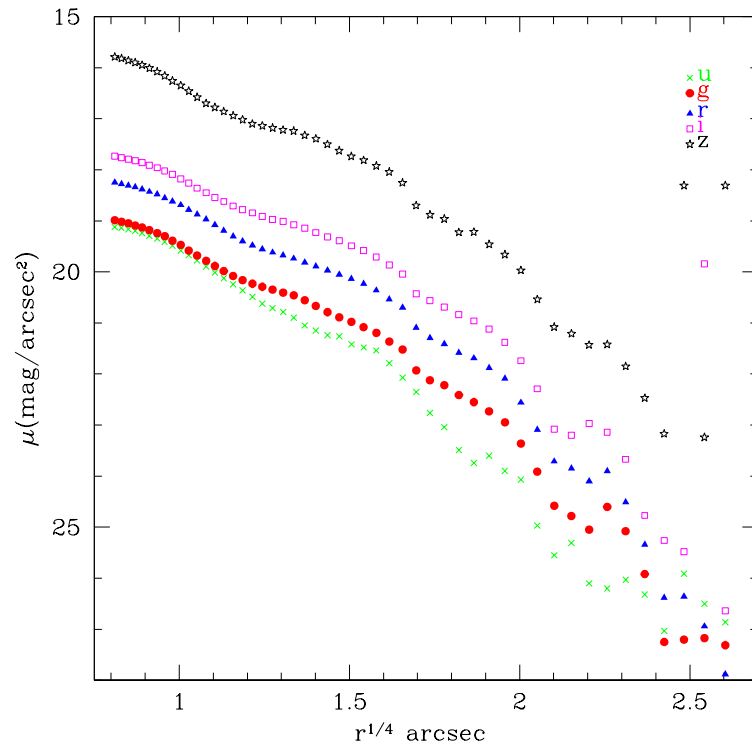


Figure 6. de Vaucouleur radial surface brightness profile. The error bar (± 0.04 for the u band, ± 0.01 for the g, r and i bands, and ± 0.02 for the z band) is within the dimensions of data points.

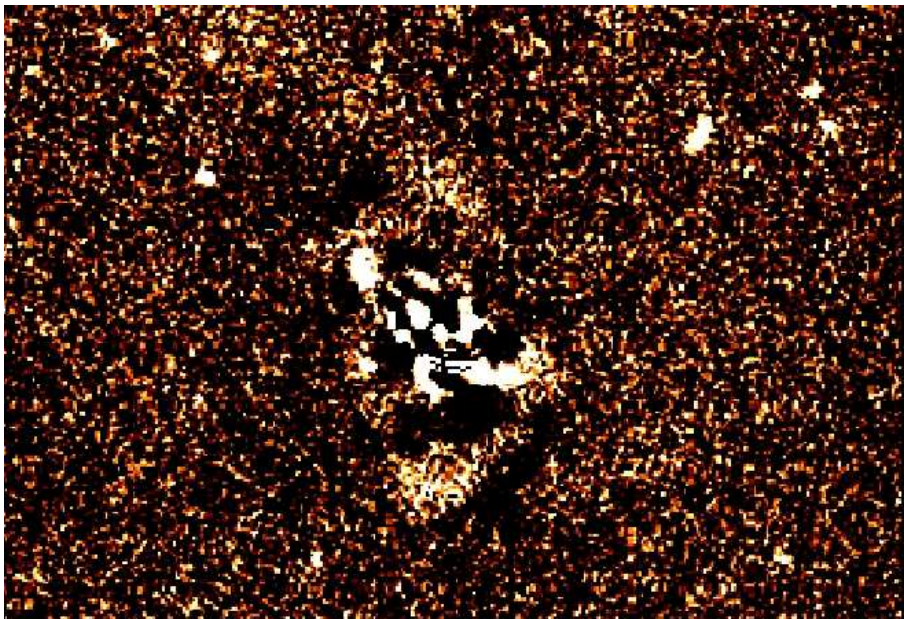


Figure 7. Residual of the subtraction of the model to the g band image.

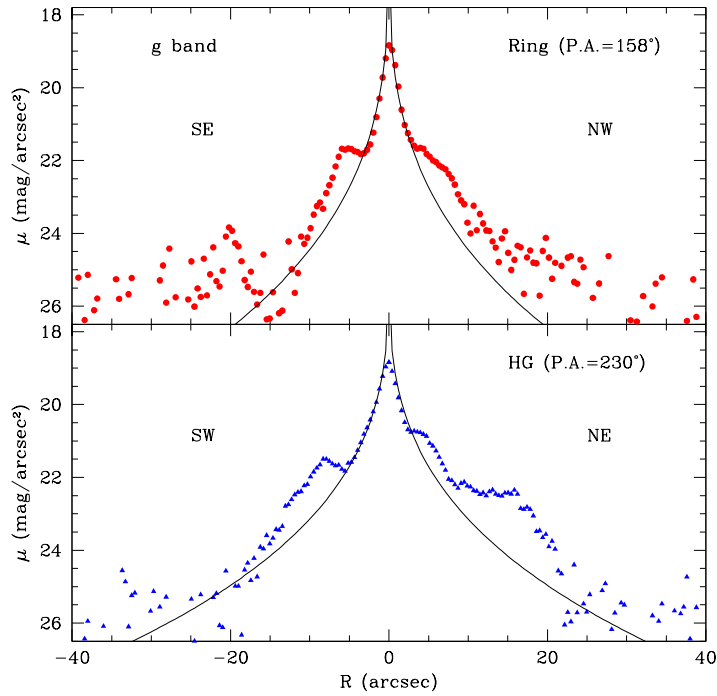


Figure 8. *Top panel* - g-band light profile along the ring-like component (P.A. 158 deg). *Bottom panel* - g-band light profile along the host galaxy (P.A. 230 deg). The black line is the 1D model of the light profile. The error bar on the surface brightness (± 0.01) is within the dimensions of data points.

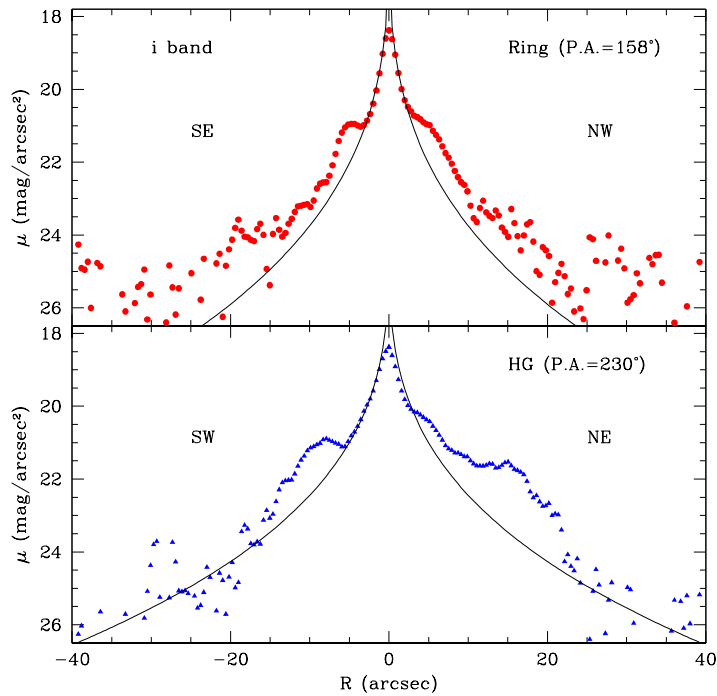


Figure 9. *Top panel* - i-band light profile along the ring-like component (P.A. 158 deg). *Bottom panel* - i-band light profile along the host galaxy (P.A. 230 deg). The black line is the 1D model of the light profile. The error bar on the surface brightness (± 0.01) is within the dimensions of data points.

by several areas of very blue colors (the nucleus, inside 4 arcsec from the center, two knots along the HG major axis and one more on the East side with respect to the galaxy nucleus), which suggest the presence of star forming regions, and this turns to be consistent with the results previously found by Beygu et al. (2013).

We also derived the integrated magnitudes and $g-r$ and $g-i$ colors in three polygons including the tail at the North-East side of VGS31b and the two sides of the ring. The polygons are determined from the g band image, using the IRAF task POLYMARK, and used for all bands. The integrated magnitudes inside each polygon are evaluated using the IRAF task POLYPHOT. The derived magnitudes and colors are reported in Table 1.

The stellar population synthesis model by Bruzual & Charlot (2003) were used to reproduce the integrated colors in the selected regions, in order to estimate the average stellar mass in the tail and in the ring-like structure of VGS31b. The key input parameters for GISSEL (*Galaxies Isochrone Synthesis Spectral Evolution Library*, Bruzual & Charlot 2003) are the Initial Mass Function (IMF), the Star Formation Rate (SFR) and the metallicity. For the ring-like structure and the tail of VGS31b, since they have bluer colors than the host galaxy, which suggest a younger age for this component, we used models with linearly declining SFR ($\psi(t) = 2M_*\tau^{-1}[1 - (t/\tau)]$) computed for metallicities of $Z=0.008$ and $Z=0.0004$, because these models reproduce the integrated colors of late-type galaxies. In every model it has been assumed that stars form according to the Salpeter (1955) IMF, in the range from 0.1 to $125 M_\odot$.

For the tail we derive a stellar mass of the order of $10^8 M_\odot$, while for the ring the estimated mass is of about $4 \times 10^8 M_\odot$. The implications of these results will be discussed in section 9.

6 EMPIRICAL OXYGEN ABUNDANCES DETERMINATION

In order to derive the oxygen abundance $12 + \log(O/H)$ and the metallicity of the ring-like structure in VGS31b, we have measured the *Oxygen abundance parameter* $R_{23} = ([OII]\lambda 3727 + [OIII]\lambda\lambda 4959 + 5007)/H\beta$ (Pagel et al. 1979), by following the procedure outlined by Spavone et al. (2010, 2011), adopted for other PRGs galaxies.

The *Empirical methods* are based on the cooling properties of ionized nebulae, which translate into a relation between emission-line intensities and oxygen abundance. Several abundance calibrators have been proposed based on different emission-line ratios: R_{23} (Pagel et al. 1979) and S_{23} (Díaz & Pérez-Montero 2000). Among the others, in this work we used the so-called P-method introduced by Pilyugin (2001).

Pilyugin (2001) realized that, for fixed oxygen abundances, the value of $X_{23} = \log R_{23}$ varies with the excitation parameter $P = R_3/R_{23}$, where $R_3 = OIII[4959+5007]/H\beta$, and proposes that this latter parameter could be used in the oxygen abundance determination. This method, called the “P-method”, proposes using a more general relation of the type $O/H = f(P, R_{23})$, than the relation $O/H = f(R_{23})$

used in the R_{23} method. The equation related to this method is

$$12 + \log(O/H)_P = \frac{R_{23} + 54.2 + 59.45P + 7.31P^2}{6.07 + 6.71P + 0.371P^2 + 0.243R_{23}} \quad (2)$$

where $P = R_3/R_{23}$. It can be used for oxygen abundance determination in moderately high-metallicity HII regions with undetectable or weak temperature-sensitive line ratios Pilyugin (2001). The definition of moderately high metallicity is adopted from Pilyugin (2001) and refers to the abundance interval $8 < 12 + \log O/H < 8.5$ where the relation $O/H = F(R_{23})$ (Pagel et al. 1979) degenerates. As suggested by Pilyugin (2001), the positions of HII regions in the $P - R_3$ diagram are related to their oxygen abundances. We use Eq. 2 above to estimate the oxygen abundances for this galaxy.

We estimated the mean oxygen abundance parameter, R_{23} , by summing the fluxes of the nebular emission lines at different regions along the ring-like structure of VGS31b (see Table 2). Such regions have been chosen by accounting the results of the 1D model of the light profile along the ring major axis, discussed in Sec 5.2: the ring is the dominant component for $r \geq 5$, but, taking into account that the HG effective radius is $r_e \sim 6.8$ arcsec, as derived by the 1D model, in order to avoid regions in which there was the “contamination” of the HG, we measured the line fluxes in the range $0 < r < 7$ arcsec for the host galaxy and $r > 7$ arcsec for the ring, obtaining a value of the oxygen abundance of $12 + \log(O/H)_P = 8.6 \pm 0.6$ for the HG and $12 + \log(O/H)_P = 8.37 \pm 0.57$ for the ring. In Table 3 we show the comparison between the average value of oxygen abundance obtained for VGS31b and those obtained for other PRGs, NGC4650A (Spavone et al. 2010), UGC7576 and UGC9796 (Spavone et al. 2011).

Given the “irregular” morphology of the ring in VGS31b, due to the presence of several “holes” inside its extension (see Fig.3), contrary to the well-defined disk-like morphology in NGC4650A, for instance, it was difficult to derive the oxygen abundance in the ring of VGS31b as a function of the radius. Thus, the available measurements let us to check that the metallicity remains almost constant along the projected major axis of the ring, except for a slight increase towards the center. The same behaviour has been observed for other PRGs (Spavone et al. 2010, 2011), unlike what it is observed for spiral galaxies, where there is a very steep gradient in metallicity.

By assuming the oxygen abundance and metallicity for the Sun to be $12 + \log(O/H)_\odot = 8.83 \pm 0.20 = A_\odot$ and $Z_\odot = 0.02$ (Grevesse & Sauval 1998), given that $Z \approx KZ_\odot$, $K_{VGS31b} = 10^{[A_{VGS31b} - A_\odot]}$, we obtain a metallicity for the ring-like structure of $Z \simeq (0.35 \pm 0.03)Z_\odot$ (see Table 3). The main implications of this analysis will be described and discussed in the following sections.

7 METALLICITY-LUMINOSITY RELATION

The mean value for the oxygen abundance along the ring-like structure of VGS31b, derived by the empirical method (see sec. 6), as a function of the total luminosity, is compared with those for different late-type galaxies by

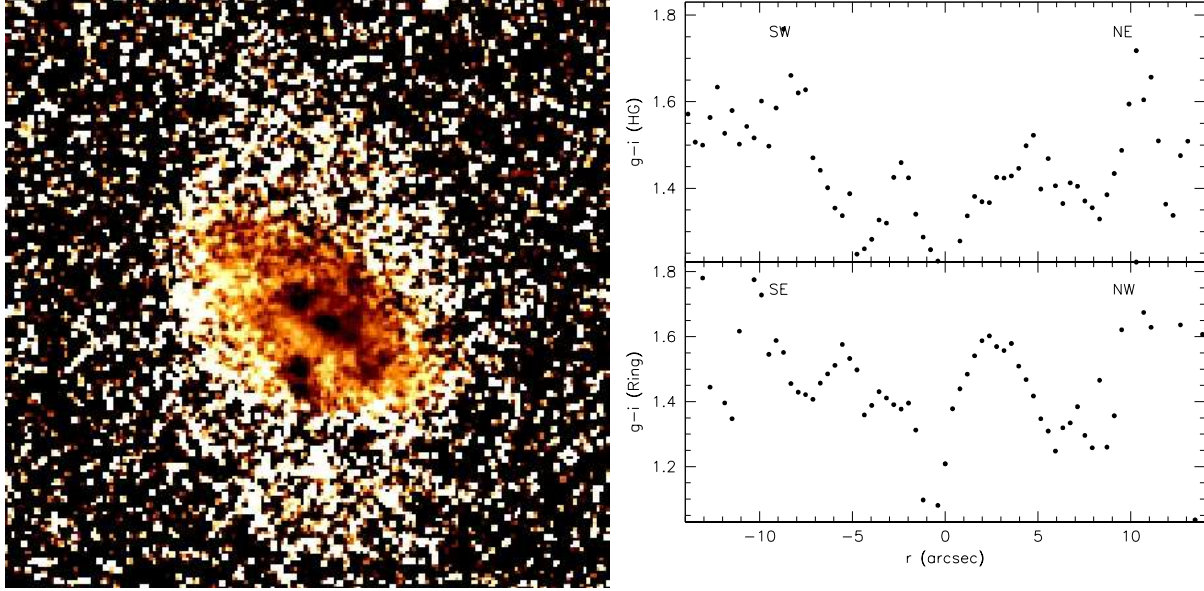


Figure 10. *Left panel* - $g-i$ color map. The North is up, while the East is on the left of the image. Lighter colors correspond to redder galaxy regions. *Right panel* - $g-i$ color profile along the major axis of the central disk galaxy (top) and along the major axis of the ring-like structure (bottom). The error bar (± 0.02) is within the dimensions of data points.

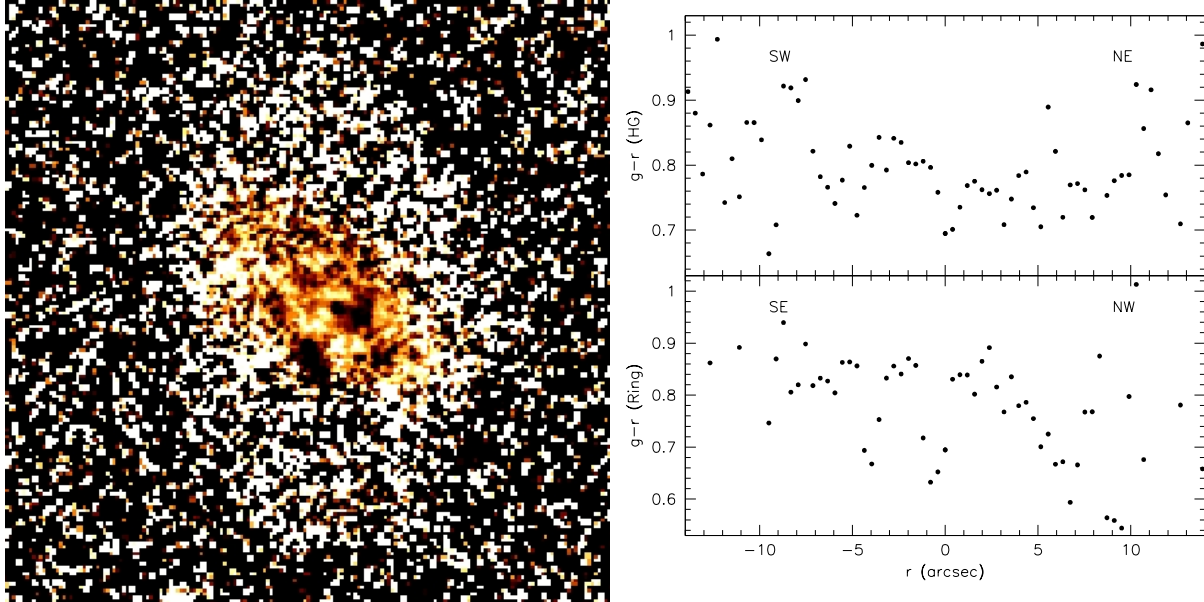


Figure 11. *Left panel* - $g-r$ color map. The North is up, while the East is on the left of the image. Lighter colors correspond to redder galaxy regions. *Right panel* - $g-r$ color profile along the major axis of the central disk galaxy (top) and along the major axis of the ring-like structure (bottom). The error bar (± 0.02) is within the dimensions of data points.

Table 1. Integrated magnitudes and colors of different regions of VGS31b.

Component	Region	$m_g(mag)$ ± 0.01	$m_r(mag)$ ± 0.01	$m_i(mag)$ ± 0.01	$g-r$ ± 0.02	$g-i$ ± 0.02
Tail	NE	18.12	17.57	16.32	0.55	1.8
Ring	N	18.12	17.20	16.19	0.92	1.9
Ring	S	18.10	17.53	16.60	0.57	1.5

Table 2. Observed and de-reddened mean emission line fluxes relative to $H\beta$.

line	λ (Å)	Observed flux relative to $H\beta$	De-reddened flux relative to $H\beta$
[OII]	3727	4.9	1.2
[OIII]	4959	2.1	2.4
[OIII]	5007	5.9	7.1
$H\gamma$	4340	1.2	0.6
$H\alpha$	6563	0.7	2.7

Table 3. Oxygen abundances and metallicities of VGS31b compared to those obtained for UGC7576, UGC9796 and NGC4650A.

Parameter	VGS31b	UGC7576	UGC9796	NGC4650A
$12 + \log(O/H)$	8.37 ± 0.57	8.5 ± 0.5	7.7 ± 1	8.2 ± 0.2
Z/Z_{\odot}	0.30 ± 0.03	0.4 ± 0.01	0.1 ± 0.005	0.2 ± 0.002

Kobulnicky & Zaritsky (1999)³ (spirals, Irregulars and HII galaxies) and several PRGs: results are shown in Fig. 12.

We found that, in the metallicity-luminosity relation, VGS31b has lower metallicity with respect to those typical for spiral galaxies of comparable total luminosity (i.e. $M_B \sim -20$), and it is located in the region where some other PRGs are found, in particular the polar disk NGC4650A (Spavone et al. 2010) and the polar ring UGC7576 (Spavone et al. 2011). Taking the total magnitude into account, such value of oxygen abundance is somewhat lower than expected by the metallicity-luminosity relation.

8 STAR FORMATION RATE

The $H\alpha$ emission is detected with adequate signal-to-noise, and from the measured integrated flux we can derive the Star Formation Rate (SFR) for the ring-like structure of VGS31b: from the $H\alpha$ luminosity, using the expression given by Kennicutt (1998), we estimate a $SFR = 7.9 \times 10^{-42} \times L(H\alpha)$. We find that it is almost constant along the ring, within a large scatter in the individual values. From the average value of $L(H\alpha) \simeq 2.5 \times 10^{39}$ erg/s we have obtained an average $SFR \sim 0.02M_{\odot}/yr$.

By using the $g-r$ integrated color and adopting the stellar population synthesis model by Bruzual & Charlot (2003), described in Sec.5.2, we estimated an upper limit for the age of VGS31b of 1Gyr. This suggests that the ring-like structure in VGS31b is even younger. Given that the last burst of star formation occurred less than 1 Gyr ago, we also checked if the present SFR and even 2 and 3 times higher (i.e. $SFR \sim 0.02M_{\odot}/yr$, $SFR \sim 0.04M_{\odot}/yr$ and $SFR \sim 0.06M_{\odot}/yr$) can give the inferred metallicities of $Z = 0.3Z_{\odot}$.

We used a linearly declining SFR (Bruzual & Charlot 2003) $\psi(t) = 2M_{\star}\tau^{-1}[1 - (t/\tau)]$ (typically used for late-type galaxies), to estimate the expected stellar mass for the three different values of the SFR and three epochs (0.8 Gyr, 1 Gyr and 2 Gyrs), obtaining stellar masses in the range

$1.3 \times 10^8 M_{\odot} \leq M_{\star} \leq 4.3 \times 10^8 M_{\odot}$. Than, by using the mass-metallicity relation derived by Tremonti et al. (2004), where $12 + \log(O/H) = -1.492 + 1.847 \log(M_{\star}) - 0.08026(\log M_{\star})^2$, we found that $0.2Z_{\odot} \leq Z \leq 0.5Z_{\odot}$. In particular, the present SFR for the ring-like structure is able to increase the metallicity of about $0.05 Z_{\odot}$ after 1Gyr. We found that the metallicity of $Z = 0.30 \pm 0.03Z_{\odot}$, estimated by using the element abundances, falls near the lower limit of the range of expected metallicities. The implications of these results will be discussed in detail in Sec. 9.

9 DISCUSSION AND CONCLUSIONS

VGS31b is a peculiar galaxy in a small group of three interacting galaxies, all embedded in a unique HI envelope, located in a void region, whose properties are very recently analysed by Beygu et al. (2013). They showed that the HI is distributed as a “filamentary structure” and some gas is accreted by the galaxies from the filament. VGS31b has a ring-like structure and a tail detected both in the optical and in the HI images. This object, as already suggested by Beygu et al. (2013), can be a good candidate for a ring formation through the cold accretion of gas along a filament, as other few cases already known (Kreckel et al. 2012; Stanonik et al. 2009).

In this work, we have presented a detailed photometric and spectroscopic study of this object, based on data extracted from SDSS and WHT archives and the main goal is to trace the possible formation history for this object. In particular, we aim to test the cold accretion of gas through a “cosmic filament” as a possible scenario for the formation of the ring-like structure in this galaxy. In the following, we address how the results obtained for VGS31b can be reconciled with the theoretical predictions for the proposed scenarios for the formation of PRGs and related objects.

The main results of the analysis performed in the present paper are:

(i) the structure of VGS31b, as appears by the optical images (see Sec.4) resembles that of forming highly-inclined ring galaxy: most of the light comes from the central spheroidal component, while the ring-like structure, inclined of about 70 degrees from the HG equatorial plane,

³ The absolute blue magnitude for the objects in the sample of Kobulnicky & Zaritsky (1999) are converted by using $H_0 = 75$ km/s/Mpc.

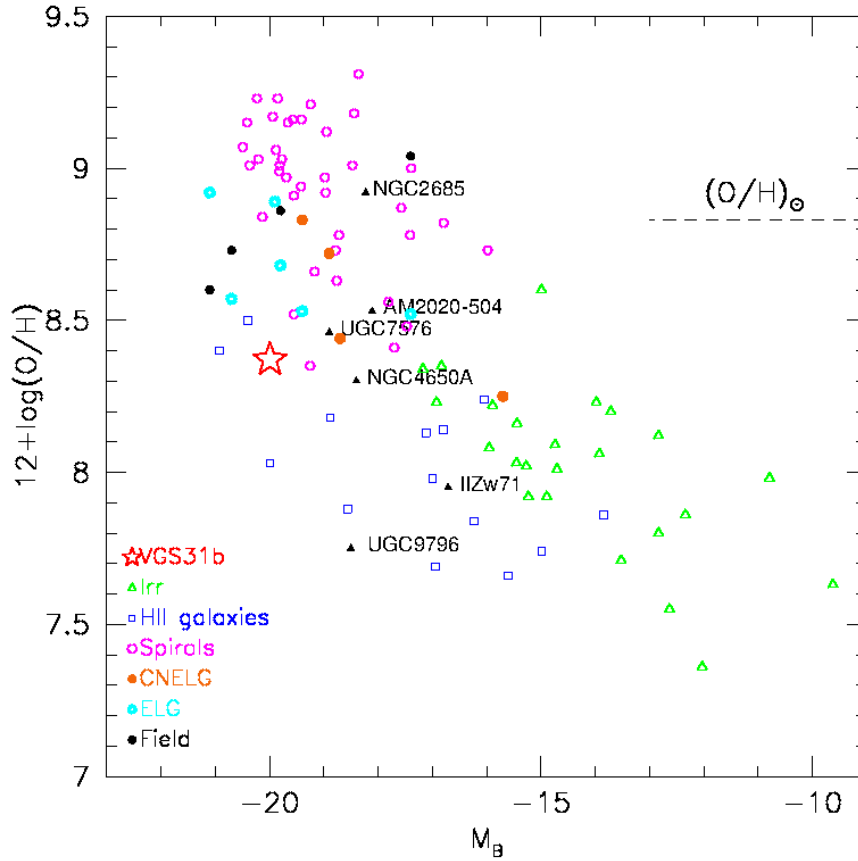


Figure 12. Oxygen abundance vs absolute blue magnitude for Compact Narrow Emission-Line Galaxies (CNELGs, orange filled circles), star-forming Emission Line Galaxies (ELGs, cyan open circles), four field galaxies with emission lines (filled black circles), nearby dwarf irregulars (open triangles), local spiral galaxies (open circles), local HII galaxies (open squares). The sample of late-type disk galaxies are by Kobulnicky & Zaritsky (1999). PRGs are: VGS31b (red star), NGC4650A (Spavone et al. 2010), IIZw71 (Pérez-Montero et al. 2009), NGC2685 (Eskridge & Pogge 1997), AM2020-504 (Freitas-Lemes et al. 2012), UGC7576 and UGC9796 (Spavone et al. 2011). The dashed line indicates the solar oxygen abundance.

and the tail, at the North-East side, become very faint towards longer wavelengths, suggesting a very young stellar population for this component;

(ii) the ring seems to reach the galaxy center tracing a “spiral-like” pattern, where the ring’s arms are connected to the two bright blobs at the ends of the bar-like structure and to the two inner arcs;

(iii) optical g-r and g-i colors show that the inner regions of the HG are characterised by several areas of very blue colors (the nucleus, inside 4 arcsec from the center, two knots along the HG major axis and one more on the East side with respect to the galaxy nucleus), which suggest the presence of star forming regions, while both the ring-like structure and the tail lack of these features: these turn to be consistent with the results previously found by Beygu et al. (2013);

(iv) The ring-like structure of VGS31b has an average metallicity of $Z = 0.3Z_{\odot}$, which is lower with respect to that of same-luminosity spiral disks, but it turns to be consistent with the values derived for other PRGs. This value remains almost constant along the whole extension of the ring;

(v) The tail at the North-East side has integrated magnitudes corresponding to stellar masses of the order of $10^8 M_{\odot}$.

The study of both the chemical abundances of HII regions in polar ring galaxies and their implications for the evolutionary scenario of these systems has been a step forward both in tracing the formation history of the galaxy and giving hints toward the mechanisms at work during the building of a disk by cold accretion process. To account both for the featureless morphology of the central spheroidal galaxy and for the more complex structure of the polar ring/disk, three main formation processes have been proposed so far: *i*) a major dissipative merger (Bekki 1997; Bekki 1998; Bournaud et al. 2005), *ii*) tidal accretion of material (gas and/or stars) from outside (Reshetnikov & Sotnikova 1997; Bournaud & Combes 2003; Hancock et al. 2009), and *iii*) cold accretion of pristine gas along a filament (Macciò et al. 2006; Brook et al. 2008; Snaith et al. 2012).

As suggested by the previous studies of PRGs (Spavone et al. 2010, 2011, 2012, Iodice et al. 2006), the critical physical parameters that can help to distinguish among the three formation scenarios are 1) the total baryonic mass (stars plus gas) observed in the polar structure with respect to the central spheroid, 2) the kinematics along both the equatorial and meridian planes, 3) the metallicity

and SFR in the polar structure.

If the polar structure around both an elliptical and disk galaxy forms by the cold accretion of gas from filaments there is no limit to the accreted mass. Moreover, due to the inflow of pristine gas, the metallicity is lower than that observed in galaxies of a comparable total luminosity, and the value derived by the present SFR is higher than those directly measured by the chemical abundances. Spavone et al. (2010, 2011) find that such predictions are consistent with observations in the polar disk galaxy NGC4650A and in the polar ring galaxy UGC7576, leading to the conclusion that the cold accretion of gas by cosmic web filaments is the most realistic formation scenario for these objects. This observational results have been confirmed by recent simulations (Snaith et al. 2012).

The tidal accretion scenario, in which gas is stripped from a gas-rich donor in a particular orbital configuration (Bournaud & Combes 2003), is able to produce polar rings and/or disks both around a disk or an elliptical galaxy. VGS31 is a small group of three interacting gas-rich galaxies in a void, thus, this scenario could be the favourite one and the close companion VGS31a could be the donor galaxy. An important constraint that need to be considered to exclude or not this scenario is the distribution of the HI gas: the three galaxies share the same envelope and they are almost aligned along a narrow filament. Thus, if the ring has formed by the tidal interaction between VSG31b and VSG31a, this observed configuration can also settled after that event, otherwise the HI distribution should be destroyed during the first galaxy encounter. Moreover, as already suggested by Beygu et al. (2013), as the mass ratio between VSG31b and VSG31a is 3 to 1, a tidal interaction would damage the disks and produce more prominent tails.

Moreover, we analysed the possibility that the disruption of a dwarf galaxy could account for the formation of the ring-like structure and the tail observed in VGS31b. As discussed in section 5.2, we used stellar population synthesis models (Bruzual & Charlot 2003) to estimate the stellar mass corresponding to the integrated magnitude observed in the tail of VGS31b. We derived a stellar mass of the order of $10^8 M_\odot$ for the tail, which turns to be higher than the typical masses of dwarf galaxies ($10^3 M_\odot \leq M_* \leq 10^7 M_\odot$, Sawala et al. 2011).

Can the ring-like structure observed in VGS31b be the result of a polar major merging between two disk galaxies already present in the filament? According to Bournaud & Combes (2003), to form a ring with a diameter of about 24 kpc, as observed in this object (see Sec.2), the relative velocities between the two galaxies should be not larger than 120 km/s and the stellar mass of the victim disk, which will form the ring, should be of the order of $10^{10} M_\odot$. Since we do not have information about the orbit of the collision, and about relative velocities, the key parameter for this scenario is the stellar mass of the remnant victim galaxy, i.e. the ring: the value estimated by the integrated colors is about $4 \times 10^8 M_\odot$, which is two order of magnitude lower than that requested in the simulation to form an extended ring as observed in VGS31b.

As already suggested by Beygu et al. (2013), the large HI amount and, most of all, its distribution let VGS31b to be a good candidate for a ring formation through the cold accretion of gas along the filament where this galaxy and its

companions are embedded in. The new result of the present work, which reinforces this view, is the low metallicity measured for the ring in VGS31b, i.e. $Z = 0.3Z_\odot$, that remains almost constant along the whole extension (see Sec.6): this turns to be consistent with the predictions by recent simulations of Snaith et al. (2012), where they found that the typical metallicity for a polar disk formed through the cold accretion of gas along a filament is about $Z = 0.2Z_\odot$ and any significant gradient is measured along the polar structure.

Given all the evidence shown above, we can conclude that the cold accretion of gas by the filament could well account for the main properties of VGS31b. Anyway, to check this scenario for the ring formation in VSG31b and exclude the other ones, one needs an ad-hoc simulation, that should reproduce both the observed properties of this object and, at the same time, the global structure observed for the whole group of galaxies. In particular, in all the simulations proposed for the PRGs formation by the cold accretion (Macciò et al. 2006; Brook et al. 2008; Snaith et al. 2012), the polar structure has the characteristic of a disk, rather than a ring: is the highly-inclined structure observed in VGS31b a disk still forming? Observations show that the tail, optical and HI, is kinematically associated to the ring and this reaches the galaxy center by tracing a “spiral-like” pattern (see Sec.4): these evidences could be consistent with an highly-inclined ring structure which is still forming, and, according to the simulations by Brook et al. (2008), it could be in the phase of the last merging through the filament, when the angular-momentum decoupling is happening.

ACKNOWLEDGEMENTS

We wish to thank the anonymous referee for helpful comments, which allow us to improve the paper. This paper makes use of data obtained from the Isaac Newton Group Archive which is maintained as part of the CASU Astronomical Data Centre at the Institute of Astronomy, Cambridge. M.S. acknowledge financial contribution from the “Fondi di Ateneo 2011” (ex 60 %) of Padua University.

REFERENCES

- Agertz O., Teyssier R., Moore B., 2009, MNRAS, 397, L64
- Arnaboldi M., Oosterloo T., Combes F., Freeman K. C., Koribalski B., 1997, AJ, 113, 585
- Bekki K., 1997, ApJL, 490, L37+
- Bekki K., 1998, ApJ, 499, 635
- Beygu B., Kreckel K., van de Weygaert R., van der Hulst J. M., van Gorkom J. H., 2013, AJ, 145, 120
- Bournaud F., Combes F., 2003, A&A, 401, 817
- Bournaud F., Elmegreen B. G., 2009, ApJL, 694, L158
- Bournaud F., Jog C. J., Combes F., 2005, A&A, 437, 69
- Brook C. B., Governato F., Quinn T., Wadsley J., Brooks A. M., Willman B., Stilp A., Jonsson P., 2008, ApJ, 689, 678
- Brosch N., Kniazev A. Y., Moiseev A., Pustilnik S. A., 2010, MNRAS, 401, 2067
- Bruzual G., Charlot S., 2003, MNRAS, 344, 1000
- Cardelli J. A., Clayton G. C., Mathis J. S., 1989, ApJ, 345, 245

- Combes F., 2011, in Brummell N. H., Brun A. S., Miesch M. S., Ponty Y., eds, IAU Symposium Vol. 271 of IAU Symposium, Galaxy Dynamics: Secular Evolution and Accretion. pp 119–126
- Cox A. L., Sparke L. S., van Moorsel G., 2006, *AJ*, 131, 828
- Dekel A., Birnboim Y., 2006, *MNRAS*, 368, 2
- Dekel A., Birnboim Y., 2008, *MNRAS*, 383, 119
- Dekel A., Birnboim Y., Engel G., Freundlich J., Goerdt T., Mumcuoglu M., Neistein E., Pichon C., Teyssier R., Zinger E., 2009, *Nature*, 457, 451
- Díaz A. I., Pérez-Montero E., 2000, *MNRAS*, 312, 130
- Edgell O. J., Lynden-Bell D., Sandage A. R., 1962, *ApJ*, 136, 748
- Elmegreen B. G., Elmegreen B. G., Ravindranath S., Coe D. A., 2007, *ApJ*, 658, 763
- Eskridge P. B., Pogge R. W., 1997, *ApJ*, 486, 259
- Freitas-Lemes P., Rodrigues I., Faúndez-Abans M., Dors O. L., Fernandes I. F., 2012, *MNRAS*, 427, 2772
- Gallagher J. S., Sparke L. S., Matthews L. D., Frattare L. M., English J., Kinney A. L., Iodice E., Arnaboldi M., 2002, *ApJ*, 568, 199
- Grevesse N., Sauval A. J., 1998, *ssr*, 85, 161
- Hancock M., Smith B. J., Struck C., Giroux M. L., Hurlock S., 2009, *AJ*, 137, 4643
- Iodice E., Arnaboldi M., De Lucia G., Gallagher III J. S., Sparke L. S., Freeman K. C., 2002, *AJ*, 123, 195
- Iodice E., Arnaboldi M., Saglia R. P., Sparke L. S., Gerhard O., Gallagher J. S., Combes F., Bournaud F., Capaccioli M., Freeman K. C., 2006, *ApJ*, 643, 200
- Iodice E., Arnaboldi M., Sparke L. S., Freeman K. C., 2002, *A&A*, 391, 117
- Katz N., Quinn T., Bertschinger E., Gelb J. M., 1994, *MNRAS*, 270, L71+
- Katz N., White S. D. M., 1993, *ApJ*, 412, 455
- Kennicutt Jr. R. C., 1998, *ARA&A*, 36, 189
- Kereš D., Katz N., Weinberg D. H., Davé R., 2005, *MNRAS*, 363, 2
- Kobulnicky H. A., Zaritsky D., 1999, *ApJ*, 511, 118
- Kreckel K., Platen E., Aragón-Calvo M. A., van Gorkom J. H., van de Weygaert R., van der Hulst J. M., Beygu B., 2012, *AJ*, 144, 16
- Macciò A. V., Moore B., Stadel J., 2006, *ApJL*, 636, L25
- Masana E., Jordi C., Maitzen H. M., Torra J., 1998, *A&A*, 128, 265
- Pagel B. E. J., Edmunds M. G., Blackwell D. E., Chun M. S., Smith G., 1979, *MNRAS*, 189, 95
- Pérez-Montero E., Díaz A. I., 2003, *MNRAS*, 346, 105
- Pérez-Montero E., García-Benito R., Díaz A. I., Pérez E., Kehrig C., 2009, *A&A*, 497, 53
- Pilyugin L. S., 2001, *A&A*, 369, 594
- Reshetnikov V., Sotnikova N., 1997, *A&A*, 325, 933
- Roškar R., Debattista V. P., Brooks A. M., Quinn T. R., Brook C. B., Governato F., Dalcanton J. J., Wadsley J., 2010, *MNRAS*, 408, 783
- Salpeter E. E., 1955, *ApJ*, 121, 161
- Sawala T., Guo Q., Scannapieco C., Jenkins A., White S., 2011, *MNRAS*, 413, 659
- Sérsic J. L., 1963, *Boletín de la Asociación Argentina de Astronomía La Plata Argentina*, 6, 41
- Snaith O. N., Gibson B. K., Brook C. B., Knebe A., Thacker R. J., Quinn T. R., Governato F., Tissera P. B., 2012, *MNRAS*, 425, 1967
- Spavone M., Iodice E., Arnaboldi M., Gerhard O., Saglia R., Longo G., 2010, *ApJ*, 714, 1081
- Spavone M., Iodice E., Arnaboldi M., Longo G., Gerhard O., 2011, *A&A*, 531, A21
- Spavone M., Iodice E., Bettoni D., Galletta G., Mazzei P., Reshetnikov V., 2012, *MNRAS*, 426, 2003
- Stanonik K., Platen E., Aragón-Calvo M. A., van Gorkom J. H., van de Weygaert R., van der Hulst J. M., Peebles P. J. E., 2009, *ApJL*, 696, L6
- Swaters R. A., Rubin V. C., 2003, *ApJL*, 587, L23
- Tremonti C. A., Heckman T. M., Kauffmann G., Brinchmann J., Charlot S., White S. D. M., Seibert M., Peng E. W., Schlegel D. J., Uomoto A., Fukugita M., Brinkmann J., 2004, *ApJ*, 613, 898
- Whitmore B. C., Lucas R. A., McElroy D. B., Steiman-Cameron T. Y., Sackett P. D., Olling R. P., 1990, *AJ*, 100, 1489

This paper has been typeset from a \TeX / \LaTeX file prepared by the author.